Twenty-Seventh Symposium (International) on Combustion/The Combustion Institute, 1998/pp. 185–191

# RATE COEFFICIENT OF H + $O_2$ + M → $HO_2$ + M (M = $H_2O$, $N_2$, Ar, $CO_2$)

PETER J. ASHMAN AND BRIAN S. HAYNES
*Department of Chemical Engineering*
*University of Sydney NSW 2006, Australia*

The oxidation of $H_2$, in the presence of NO, has been studied using a laminar flow reactor for the temperature range 750–900 K with residence times of the order of 1–2 s. Product species concentrations are determined using a chemiluminescent $NO_x$ analyzer ($NO_x$ and NO), FTIR spectrometer ($H_2O$), and a micro–gas chromatograph ($H_2$).

The chemical-kinetic model prediction for $NO_2$ is sensitive to only a small number of rate constants of which only the value of $k_5$ (H + $O_2$ + M → $HO_2$ + M) is uncertain. Matching of the experimental and predicted $NO_2$ profiles is then performed using the value of $k_5$ as an adjustable parameter, leading to an experimental determination of $k_5$. The effect of different third bodies ($N_2$, $CO_2$, Ar, and $H_2O$) on the rate of $k_5$ is investigated by the use of $N_2$, $CO_2$, Ar, and moist $N_2$ carrier gases.

The value of $k_5$ (M = $N_2$) has been determined as $k_{5,N_2} = 2.25 \times 10^{15} \exp(+680/T)$ cm$^6$ mol$^{-2}$ s$^{-1}$ (±30%) in the temperature range 750–900 K. Comparison of this value for $k_5$ (M = $N_2$) with values determined for $M$ = $H_2O$, $CO_2$, and Ar lead to third-body efficiencies (relative to $N_2$) for these species of 10.6, 2.4, and 0.56, respectively, throughout the temperature range studied.

## Introduction

Termolecular recombination reactions are an important class of reaction that dominate the postflame chemistry of hydrogen, carbon monoxide, and other flames [1] and are also responsible for the bulk of the energy release associated with combustion. The rate of the chain-terminating recombination reaction R.5 relative to that of the chain-branching reaction R.3 is a determining factor in the ignition chemistry of hydrocarbon/oxygen systems. (Reaction numbers are taken from Bromly et al. [2]). The production of $HO_2$ radicals via reaction R.5 leads to the emission of $NO_2$ from indoor gas appliances [3] and gas turbine exhausts [4]. In the atmosphere, reaction R.5 is the major route for the conversion of free H to $HO_2$ and hence contributes in ozone photochemical cycles.

$$H + O_2 + M \rightarrow HO_2 + M \qquad (R.5)$$

$$H + O_2 \rightarrow OH + O \qquad (R.3)$$

The third-body efficiency for $H_2O$ in reaction R.5 is reported to be up to 15 times that of $N_2$ [5,6]. Hence, the rate of reaction R.5 is particularly sensitive to composition.

Ashmore and Tyler [7] observed that in $H_2/O_2$ systems containing small amounts of NO, a pseudo–steady state is reached at sufficiently high NO/$O_2$ ratios. At this steady-state condition, the concentration of $NO_2$ (formed by reaction R.34) is given by equation 1. It can be seen from Eq. 1 that the $NO_2$ concentration is independent of the initial NO concentration and is decoupled from the $H_2/H_2O$ system. By measuring $[NO_2]/[O_2]$ as a function of [M] they determined values of the ratio $k_5/k_{35}$ for a range of third bodies ($H_2$, $O_2$, $H_2O$, $N_2$, $CO_2$, and He) at 633 K.

$$NO + HO_2 \rightarrow NO_2 + OH \qquad (R.34)$$

$$NO_2 + H \rightarrow NO + OH \qquad (R.35)$$

$$[NO_2] = \frac{k_5[M]}{k_{35}} [O_2] \qquad (1)$$

An experimental and modeling study of the NO-sensitized oxidation of $H_2$ by Bromly et al. [2] confirmed the major findings of Ashmore and Tyler [7]. In particular, computer modeling showed that the predicted value for $[NO_2]$ in the plateau region is sensitive only to the estimates of the rate coefficients for R.5 (logarithmic sensitivity coefficient, $S_{NO_2,5} \rightarrow +1$) and R.35 ($S_{NO_2,35} \rightarrow -1$). By obtaining a fit of their kinetic model to the experimental data, using $k_5$ (M = $N_2$) as the adjustable parameter, Bromly et al. [2] obtained an estimate for $k_{5,N_2}$, in the temperature range 700 to 825 K, with an absolute uncertainty of <35%.

The focus of this paper is to extend the work of Bromly et al. [2], by the addition of $H_2O$ (0%–20%) to the $N_2$ carrier gas, to determine a value for $k_{5,H_2O}$ and to compare the value of $k_{5,N_2}$ determined here with the value of Bromly et al. [2]. The efficiency of $CO_2$ and of Ar as third-body partners is also investigated.

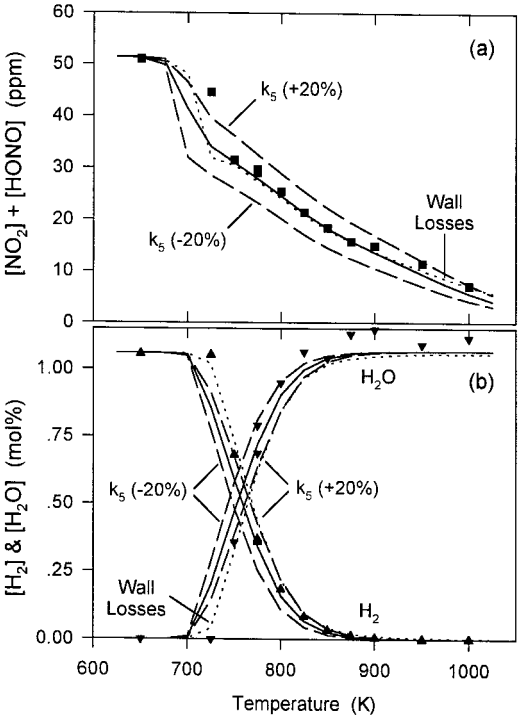


FIG. 1. (a) $[NO_2]$ + [HONO] (■) and (b) $[H_2]$ (▲) and $[H_2O]$ (▼) for the reaction of 1.06% $H_2$, 3.2% $O_2$, and 101 ppm $NO_x$ in a $N_2$ carrier gas. Residence time = 1.1 s (calculated at 773 K). Solid, dashed, and dotted lines are model predictions—see text for details.

## Experimental

The experimental apparatus consists of a 210 $cm^3$ silica laminar flow reactor housed in a temperature-controlled, fan-stirred oven. The reactor has two 4.5-mm i.d. preheat coils of 1.5 m and 3.5 m in length, a short mixing section, and an 8-mm i.d. reaction section of 4.5 m in length. The total flow through the reactor (at STP) was held constant and, for experiments in which temperature was varied, changes in residence time with temperature were accounted for in the kinetic modeling. Residence times were typically in the range 0.7–2.2 s. Flow rates of the reactant gases were metered using mass flow controllers to give the desired inlet concentration. Typical inlet concentrations are $H_2$ = 1%, $O_2$ = 3%, and NO = 60–180 ppm.

Nitrogen carrier gas was mixed with a small flow of pure $H_2$ prior to $H_2O$ addition. Water was added by passing the carrier gas through a 3-mm i.d. × 1.5-m tube constructed of a hygroscopic, ion-exchange membrane that was contained within a water bath. The water bath was bypassed for experiments without $H_2O$ addition. The $H_2O$ concentration in the inlet stream was controlled using the temperature of the water bath. The moist carrier gas stream entered the reactor through a heated transfer line and then through the main silica preheat coil. Pure $O_2$ and NO (1% in $N_2$) entered through the second silica preheat coil. Due to the long residence time within the transfer line (ca. 60 s) and the high NO and $O_2$ concentrations in this stream, some conversion of NO to $NO_2$ occurred prior to the reactor inlet. Modeling studies show that the final $NO_2$ concentration is independent of the inlet $NO/NO_2$ ratio for the conditions used in this experiment. The reactor products passed through a short, insulated transfer line prior to dilution with a large flow (40 standard $l.min^{-1}$) of dry air. This dilution was performed in order to reduce the dew point of the product stream below ambient and prevent condensation in the sampling lines.

Some experiments, without $H_2O$ addition, were conducted in which the carrier gas ($N_2$, $CO_2$, or Ar) is mixed with $O_2$ and NO (1% NO in $N_2$) and enters through the main preheat coil. A small flow of pure $H_2$ enters through the smaller preheat coil. Product gases exit the reactor and are quenched in a water-cooled condenser. These experiments are not shown explicitly in this paper but the results have been included in the determination of $k_5$.

The concentration of $NO_x$ ($NO_x$ = NO + $NO_2$ + HONO) and NO, were determined using a chemiluminescent $NO_x$ analyzer (Model 200, Advanced Pollution Instrumentation). A small flow of the reaction products was diluted with $N_2$ using mass flow controllers to reduce the concentration of $NO_x$ to below 1 ppm before transfer to the $NO_x$ analyzer. An FTIR spectrometer (FTS40, Bio-Rad) was used to determine the concentration of $H_2O$ using the peak height at 2041.6 $cm^{-1}$, or, in the presence of high CO concentrations, the peak height at 1988.7 $cm^{-1}$. A micro-gas chromatograph (M200, MTI Analytical Instruments) was used to determine the concentration of $H_2$.

Computer-kinetic modeling of the reactions was carried out using the Sandia SENKIN/CHEMKIN II package [8,9] and the Sandia thermodynamic database [10]. We have used the reaction mechanism of Bromly et al. [2]. Some production of CO occurs when $CO_2$ is used as a carrier gas and so reactions involving CO and $CO_2$ have been included in the mechanism. The reactions included are reactions R.218–R.223 from the mechanism of Bromly et al. [11].

## Results

In Fig. 1a, the apparent $NO_2$ concentration is shown as a function of temperature for the reaction of 1.06% $H_2$, 3.2% $O_2$, and 101 ppm $NO_x$($NO_2/NO_x$ = 0.5) in a $N_2$ carrier gas at a residence time

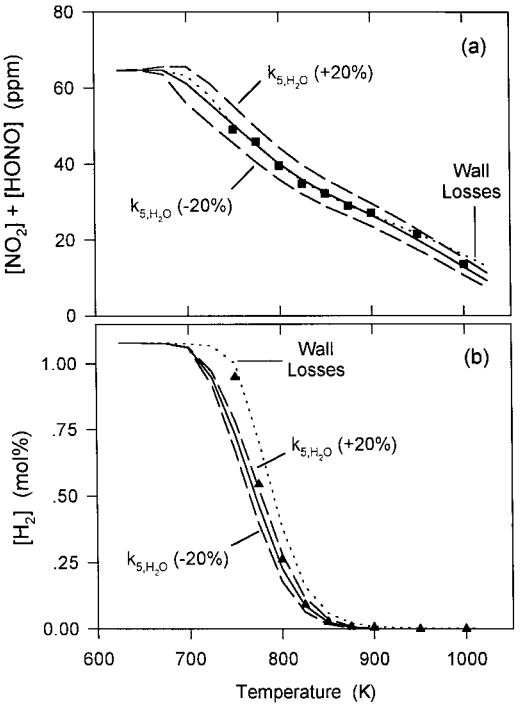


FIG. 2. (a) $[NO_2]$ + [HONO] (■) and (b) $[H_2]$ (▲) for the reaction of 1.08% $H_2$, 3.1% $O_2$, and 96 ppm $NO_x$ in a 8.7% $H_2O$ in $N_2$ carrier gas. Residence time = 2.17 s (calculated at 773 K). Solid, dashed, and dotted lines are model predictions—see text for details.

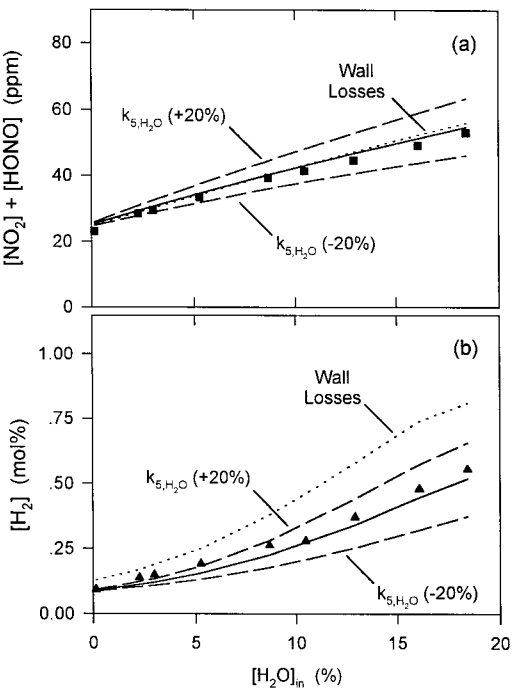


FIG. 3. (a) $[NO_2]$ + [HONO] (■) and (b) $[H_2]$ (▲) for the reaction of 1.08% $H_2$, 3.1% $O_2$, and 95 ppm $NO_x$ in a moist $N_2$ carrier gas at 800 K. Residence time = 2.1 s (calculated at 773 K). Solid, dashed, and dotted lines are model predictions—see text for details.

of 1.1 s (calculated at 773 K). The experimental apparent $NO_2$ concentration is obtained as the difference between the $NO_x$ and NO concentrations given by the chemiluminescent $NO_x$ analyzer, whereas the modeling results are obtained as the sum of the predicted $NO_2$ and HONO concentrations. In Fig. 1b, the concentrations of $H_2$ and $H_2O$ are plotted against temperature for the same experiment.

In Fig. 1–3, the solid lines are the model predictions obtained using the mechanism of Bromly et al. [2] together with our value for $k_5$. The dashed lines in Fig. 1 are model predictions where the value of $k_5$ was varied by ±20%. The dashed lines in Fig. 2 and 3 are model predictions where the value of $k_{5,H_2O}$ was varied by ±20% with the value for $k_{5,N_2}$ held constant. The dotted lines labeled "wall losses" in Fig. 1–3 show the effect on the calculated species profiles when $HO_2$, OH, O, and H radicals are consumed at the walls of the reactor at the mass-transfer limited rate. The calculation of these rates are discussed in the next section.

In Fig. 2a, the apparent $NO_2$ concentration is shown as a function of temperature for the reaction of 1.08% $H_2$, 3.1% $O_2$, and 96 ppm $NO_x$ ($NO_2/NO_x$ = 0.68) in a carrier gas of 8.7% $H_2O$ in $N_2$ at a residence time of 2.17 s (calculated at 773 K). In Fig. 2b, the results for $[H_2]$ are plotted against temperature for the same experiment. The experimental and calculated results for the apparent $NO_2$ concentration are determined as for Fig. 1.

Figure 3 shows results for the reaction of 1.08% $H_2$, 3.1% $O_2$, and 95 ppm $NO_x$($NO_2/NO_x$ = 0.67) at a temperature of 800 K where the concentration of $H_2O$ in the $N_2$ carrier gas is varied in the range 0%–18.4% at a residence time of 2.1 s. The experimental and calculated results for the apparent $NO_2$ concentration are shown in Fig. 3a as a function of the inlet $H_2O$ concentration and are determined in the same manner as for Fig. 1 and 2. In Fig. 3b, the concentration of $H_2$ is plotted against inlet $H_2O$ concentration for the same experiment.

## Discussion

As shown by Bromly et al. [2], the model predictions for $[NO_2]$ in this system are sensitive only to the values of $k_5$ ($S_{NO_2,5} = \partial \ln[NO_2]/\partial \ln A_5 = +1$)

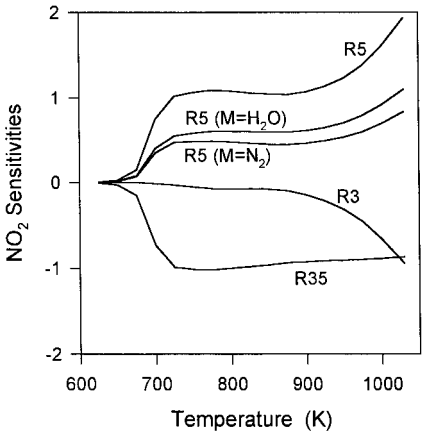


FIG. 4. Sensitivity coefficients ($S_{ij} = \partial \ln x_i / \partial \ln A_j$) for the formation of $NO_2$ at the conditions shown in Fig. 2 (1.08% $H_2$, 3.1% $O_2$, 96 ppm $NO_x$, 8.7% $H_2O$ in $N_2$; residence time = 2.17 s).

and $k_{35}$ ($S_{NO_2,35} = -1$). The rate constant for reaction R.35 is well known and hence the prediction of $[NO_2]$ is sensitive to only one uncertain parameter, namely $k_5$. Following the method of Bromly et al. [2], matching of the experimental and predicted $[NO_2]$ profiles is then performed using the value of $k_5$ as an adjustable parameter, leading to an experimental determination of $k_5$.

The contributions of the reactant and product species as third bodies in reaction R.5 is minor and $k_5$ is dominated by the contribution from the carrier gas. The use of pure $H_2O$ as a carrier gas is experimentally difficult to achieve and $H_2O$ is such a strong promoter of reaction R.5 that the system behaves quite differently. For these reasons, dilute mixtures of $H_2O$ in $N_2$ are used as the carrier gas when determining $k_{5,H_2O}$. Figure 4 shows the normalized mole fraction sensitivity coefficients ($S_{ij} = \partial \ln x_i / \partial \ln A_j$) for the prediction of $NO_2$ concentration for the reaction conditions corresponding to Fig. 2. Shown separately are the sensitivities of the predicted $NO_2$ concentration to $k_{5,N_2}$ and $k_{5,H_2O}$, which sum together to give the total sensitivity to the rate of reaction R.5. Analysis of this system leads to conclusions similar to those of Bromly et al. [2]—the predicted $NO_2$ concentration is sensitive only to a small number of rate constants, $k_{35}$, $k_{5,N_2}$ and $k_{5,H_2O}$, of which, only $k_{5,H_2O}$ is uncertain in that $k_{5,N_2}$ is known from the results shown in Fig. 1. Hence, matching of the experimental and predicted $NO_2$ concentration profiles using the value of $k_{5,H_2O}$ as an adjustable parameter leads to an experimental determination of $k_{5,H_2O}$.

Comparison of experimental and predicted $NO_2$ concentrations is not trivial, and a number of issues need to be addressed. Chemiluminescent $NO_x$ analyzers typically determine the total $NO_x$ concentration by passing the sample through a converter that reduces $NO_2$ to NO. A separate determination of the NO concentration is made using a portion of the sample that has bypassed the converter. In this work, small amounts of nitrous acid (HONO) are present in the sample which is also reduced to NO in the converter. Hence, the difference between the $NO_x$ and NO concentrations, which is reported by the analyzer as the concentration of $NO_2$, is in fact an apparent $NO_2$ concentration equal to the sum of the $NO_2$ and HONO concentrations. The predicted concentrations of HONO never exceed 5 ppm and in most cases are significantly less. The measurement of HONO using the FTIR is difficult in most circumstances, given the small concentrations of HONO and the presence of large concentrations of $H_2O$, and is impossible for experiments involving $H_2O$ addition. It is also difficult to sample HONO quantitatively due to the effect of surface catalyzed reactions.

The output of the chemical-kinetic model predicts species concentrations at the reaction temperature. Typically, small amounts of $HO_2$, and at higher temperatures OH radicals, are present that are unstable at ambient temperatures. These radicals will be converted to stable species during the quenching process. The fate of these radicals has been investigated computationally and was found to influence the concentrations of both $NO_2$ and HONO. The quenching mechanism involves the destruction of $HO_2$ almost exclusively via reaction R.34 producing $NO_2$ and OH. The OH formed via R.34 together with that already present is consumed via a number of reactions including R.39 and the effect of quenching on the predicted apparent $NO_2$ concentration profiles depends on what fraction of OH is consumed via this reaction. We have defined a term $NO_2^*$ (given by Eq. 2) representing the maximum possible effect of quenching on the predicted apparent $NO_2$ concentration, in which all OH is consumed via reaction R.39. At the conditions used in this study, the concentration of $NO_2^*$ and the apparent $NO_2$ concentration differ by less than a few percent.

$$NO + HO_2 \rightarrow NO_2 + OH \qquad \text{(R.34)}$$

$$NO + OH\ (+M) \rightarrow HONO\ (+M) \qquad \text{(R.39)}$$

$$[NO_2^*] = [NO_2] + [HONO] + 2[HO_2] + [OH] \qquad (2)$$

The dotted lines in Fig. 1–3 show that the loss of radical species at the reactor surface has a negligible impact on the prediction of the apparent $NO_2$ concentration under most conditions. In the regions where the effect is likely to be significant, generally at temperatures >900 K, the results are excluded in

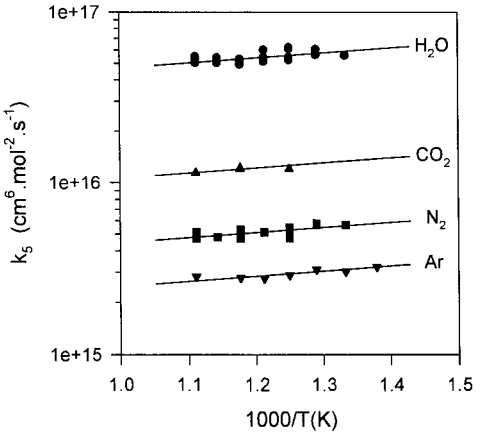


FIG. 5. Rate constants for $k_5$ (H + $O_2$ + M → $HO_2$ + M) for M = $N_2$ (■), $H_2O$ (●), $CO_2$ (▲), and Ar (▼) determined experimentally from data including that shown in Fig. 1–3. Lines are Arrhenius fits to the data using the negative activation energy (M = $N_2$) of Hsu et al. [16].

the determination of $k_5$. The rate of destruction of $HO_2$, OH, O, and H radicals is assumed to be limited by the rate of diffusion of these species to the wall. First-order rate constants are calculated, following the method of Thomas et al. [12], based on a cylindrical channel model assuming laminar flow and are given by equation 3:

$$k_i = (3/2)\theta^2 D_i \quad (3)$$

where $k_i$ is the first-order rate constant ($s^{-1}$), $\theta$ is the surface-to-volume ratio of the reactor (500 $m^2/m^3$ for this reactor), and $D_i$ is the molecular diffusivity of species $i$ ($m^2/s$). Molecular diffusivities for the radicals species are estimated using the method of Fuller et al. [13]. The model predictions for the concentration of $H_2$ are more strongly influenced by the inclusion of radical wall losses (Fig. 1–3). However, the experimental concentration profiles for $H_2$ are usually shifted only slightly toward the values predicted by the loss of radicals at the wall because the assumption of a mass-transfer limited rate provides only an upper limit to the extent of wall losses and is not intended to accurately account for surface effects.

Chemical-kinetic modeling is performed assuming simple plug flow through the reactor. The assumption that radial and axial dispersion is negligible has been verified using the analyses of Mulcahy and Pethard [14] and Wan and Ziegler [15]. At the conditions used in this study, the time required for radial variations in concentration to be eliminated by diffusion is in the range 1–25 ms which is much faster than the residence time in the reactor. Peclet numbers are in the range 100–8000 which are sufficiently high that differences between a dispersion model and a plug flow model are negligible. Furthermore, it is a characteristic of the $NO_2$ results, and hence of the values determined for $k_5$, that they are relatively independent of residence time under our conditions.

The values determined for $k_5$, M = $H_2O$, $N_2$, $CO_2$, and Ar, are presented in Arrhenius form in Fig. 5. The temperature range (750–900 K) is quite small; however, $k_5$ clearly increases with decreasing temperature, and a negative activation energy of 5.7 kJ/mol, as determined by Hsu et al. [16] for M = $N_2$, provides a reasonable description of the trend in the experimental data. The results for $k_{5,N_2}$ shown in Fig. 5 are determined using the data shown in Fig. 1 together with a repeat of this experiment using the alternate inlet configuration described previously in the experimental section of this paper. Also included are data from three experiments conducted at temperatures of 800, 850 and 900 K in which the inlet concentration of NO was varied in the range 80–170 ppm. The value for $k_{5,N_2}$ (750–900 K) determined from the data in Fig. 5 is $k_{5,N_2} = 2.25 \times 10^{15} \exp(+680/T)$ $cm^6$ $mol^{-2}$ $s^{-1}$. This value is 13% lower than that determined by Bromly et al. [2] which is within the relative experimental uncertainties for these two studies. As discussed by Bromly et al. [2], the absolute uncertainty in $k_{5,N_2}$ is estimated to be <30%.

The results for $k_{5,H_2O}$ shown in Fig. 5 are determined using the data shown in Fig. 2 and Fig. 3 together with data from two additional experiments that have not been presented due to space limitations. The additional experiments were conducted at the same conditions as those for Fig. 2 except that in the first experiment the inlet concentration of $H_2O$ was increased to 16.7% and in the second experiment the residence time was decreased to 0.94 s (calculated at 773 K). The value for $k_{5,H_2O}$ (750–900 K) determined from the data in Fig. 5 is $k_{5,H_2O} = 2.38 \times 10^{16} \exp(+680/T)$ $cm^6$ $mol^{-2}$ $s^{-1}$ with an estimated absolute uncertainty similar to that for $k_{5,N_2}$ (±30%). The average third-body efficiency for $H_2O$ relative to $N_2$ is therefore found to be 10.6 ± 1 over the temperature range 750–900 K. The uncertainty in this relative efficiency is substantially less than that in the absolute values of the individual rate coefficients due to the incremental effect of $H_2O$ relative to $N_2$, which can be observed directly in analyses such as those shown in Fig. 3.

Also shown in Fig. 5 are results for $k_{5,CO_2}$ and $k_{5,Ar}$ determined using data from experiments (not presented here) that are similar to that shown in Fig. 1 but using $CO_2$ and Ar carrier gases. The $CO_2$ results also include data from an experiment conducted at 850 K in which the inlet concentration of NO was varied in the range 70–180 ppm. The values for $k_{5,CO_2}$ (800–900 K) and $k_{5,Ar}$ (725–900 K) determined from the data in Fig. 5 lead to third-body efficiencies for $CO_2$ and Ar (relative to $N_2$) in

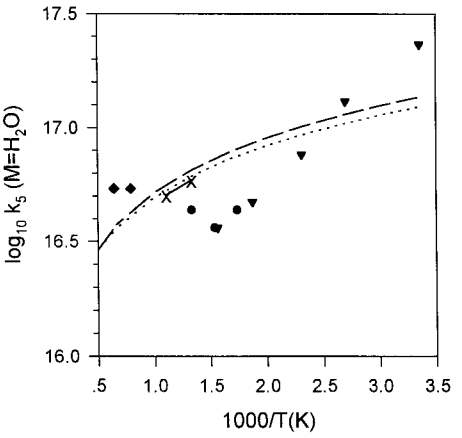


FIG. 6. Comparison of rate constants for $k_{5,H_2O}$ ($H + O_2 + H_2O \rightarrow HO_2 + H_2O$) from this work (X); Hsu et al. [16] (▼); Carleton et al. [17] (●); Getzinger and Blair [18] (◆); Warnatz [6] (–––·); and GRI-Mech [19] (------).

reaction R.5 of 2.4 and 0.56, respectively, when compared with the value of $k_{5,N_2}$.

Figure 6 compares our results for $k_{5,H_2O}$ with experimental values reported by others [16–18] together with the recommendation of Warnatz [6] and the value used in the GRI-Mech mechanism [19]. Our results agree well with the recommendation of Warnatz [6] and the GRI-Mech value [19]. The large degree of experimental uncertainty reported for the high-temperature value of Carleton et al. [17] overlaps with our result. However, the high-temperature result is inconsistent with their low-temperature results which agree with the results of Hsu et al. [16]. Although the temperature dependence of Hsu et al. [16] for $M = N_2$ fits the weak temperature dependence exhibited by our results, extrapolation of their $M = H_2O$ data to our higher temperatures gives values for $k_{5,H_2O}$ that are 50% lower than our value at 825 K. The results of Getzinger and Blair [18] were obtained at much higher temperatures and are difficult to compare with our results.

In addition to the absolute values of $k_{5,H_2O}$ shown in Fig. 6, a number of relative values of $k_{5,H_2O}$ have been reported in the literature. Ashmore and Tyler [7] report third-body efficiencies for $H_2O$ and $N_2$ (relative to $H_2$) of 6.6 and 0.55 at 633 K, leading to a third-body efficiency for $H_2O$ relative to $N_2$ of 12. Baldwin and co-workers [20,21] report third-body efficiencies for $H_2O$ and $N_2$ (relative to $H_2$) of 6.4 and 0.43 in the temperature range 733–813K, leading to a third-body efficiency for $H_2O$ relative to $N_2$ of 14.9.

The latest recommendation for $k_{5,H_2O}$ by Baulch et al. [22] has not been included in Fig. 6 as we believe that an error exists with this number that has not been previously reported as an erratum. Comparison of the Baulch et al. [22] value for $M = H_2O$ with their value for $M = N_2$ results in a third-body efficiency for $H_2O$ (relative to $N_2$) of only 1.1 which is clearly incorrect. Increasing the Baulch et al. [22] recommendation by a factor of 10 gives a value for $k_{5,H_2O}$ that is 30% higher than the value determined in this work.

Our result for $k_{5,Ar}$ agrees well with the Baulch et al. recommendation [23] and the most recent experimental determination of $k_{5,Ar}$ by Davidson et al. [24]. Experimental results for $k_{5,CO_2}$ exist only for temperatures below 100 °C, and the Baulch et al. compilation [22,23] does not make an explicit recommendation for this rate constant. The GRI-Mech mechanism [19] uses a value for $k_{5,CO_2}$ that is less than 10% higher than the value reported here.

## Conclusions

Comparison of predicted and experimental values for the concentration of $NO_2$ in the $H_2/O_2/NO$ system allows rate constants for $H + O_2 + M \rightarrow HO_2 + M$ ($M = N_2$, $H_2O$, $CO_2$, Ar) to be determined. The value of $k_{5,N_2}$ has been determined as $k_{5,N_2} = 2.25 \times 10^{15} \exp(+680/T)$ cm$^6$ mol$^{-2}$ s$^{-1}$ ($\pm 30\%$) in the temperature range 750–900 K. Comparison of this value for $k_5$ ($M = N_2$) with values determined for $M = H_2O$, $CO_2$, and Ar lead to third-body efficiencies (relative to $N_2$) for these species of 10.6, 2.4, and 0.56, respectively.

*Acknowledgments*

This work has been supported by the Australian Research Council.

REFERENCES

1. Gardiner Jr., W. C. and Troe, J., in *Combustion Chemistry*, (W. C. Gardiner Jr., ed.), Springer Verlag, New York, 1984, chapter 4.
2. Bromly, J. H., Barnes, F. J., Nelson, P. F., and Haynes, B. S., *Int. J. Chem. Kinet.* 27:1165–1178 (1995).
3. Bromly, J. H., Barnes, F. J., Mandyczewsky, R., Edwards, T. J., and Haynes, B. S., in *Twenty-Fourth Symposium (International) on Combustion.* The Combustion Institute, Pittsburgh, 1992, pp. 899–907.
4. Haynes, B. S., in *The First Asia-Pacific Conference on Combustion.* The Combustion Institute, Pittsburgh, 1997, pp. 94–97.
5. Miller, J. A. and Bowman, C. T., *Prog. Energy Combust. Sci.* 15:287–338 (1989)
6. Warnatz, J., in *Combustion Chemistry* (W. C. Gardiner Jr., ed.), Springer Verlag, New York, 1984, p. 199.
7. Ashmore, P. G. and Tyler, B. J., *Trans. Faraday Soc.* 58:1108–1116 (1962).

8. Kee, R. J., Rupley, F. M., and Miller, J. A., "CHEMKIN-II: A Fortran Chemical Kinetics Package for the Analysis of Gas-Phase Chemical Kinetics," Sandia National Laboratories report SAND89-8009.
9. Lutz, A. E., Kee, R. J., and Miller, J. A., "SENKIN: A Fortran Program for Predicting Homogeneous Gas-Phase Chemical Kinetics with Sensitivity Analysis," Sandia National Laboratories report SAND87-8248.
10. Kee, R. J., Rupley, F. M., and Miller, J. A., "The CHEMKIN Thermodynamic Database," Sandia report 87-8215.
11. Bromly, J. H., Barnes, F. J., Muris, S., You, X., and Haynes, B. S., *Combust. Sci. Tech.* 115:259–296 (1996).
12. Thomas, D. J., Willi, R., and Baiker, A., *Ind. Eng. Chem. Res.* 31:2272–2278 (1992).
13. Fuller, E. N., Schettler, P. D., and Giddings, J. C., *Ind. Eng. Chem.* 58(5):19–27 (1966).
14. Mulcahy, M. F. R. and Pethard, M. R., *Aust. J. Chem.* 16:527–543 (1963).
15. Wan, C-G. and Ziegler, E. N., *Chem. Eng. Sci.* 25:723–727 (1970).
16. Hsu, K.-J., Anderson, S. M., Durant, J. L., and Kaufman, F., *J. Phys. Chem.* 93:1018–1021 (1989).
17. Carleton, K. L., Kessler, W. J., and Marinelli, W. J., *J. Phys. Chem.* 97:6412–6417 (1993).
18. Getzinger, R. W. and Blair, L. S., *Combust. Flame* 13:271–284 (1969).
19. Bowman, C. T., Hanson, R. K., Gardiner Jr., W. C., Lissianski, V., Frenklach, M., Goldenberg, M., and Smith, G. P., "GRI-Mech 2.11—An Optimized Detailed Chemical Reaction Mechanism for Methane Combustion and NO Formation and Reburning," GRI Report GRI-97/0020, March 1997. (The most recent version of this report is available at http://www.me.berkeley.edu/gri_mech/.)
20. Baldwin, R. R. and Brooks, C. T., *Trans. Faraday Soc.* 58:1782–1788 (1962).
21. Baldwin, R. R. and Walker, R. W., *Essays in Chemistry* 3:1–37 (1972).
22. Baulch, D. L., Cobos, C. J., Cox, R. A., Esser, C., Frank, P., Just, Th., Kerr, J. A., Pilling, M. J., Troe, J., Walker, R. W., and Warnatz, J., *J. Phys. Chem. Ref. Data.* 21:411–429 (1992).
23. Baulch, D. L., Cobos, C. J., Cox, R. A., Frank, P., Hayman, G., Just, Th., Kerr, J. A., Murrells, T., Pilling, M. J., Troe, J., Walker, R. W., and Warnatz, J., *Combust. Flame* 98:59–79 (1994).
24. Davidson, D. F., Petersen, E. L., Röhrig, M., Hanson, R. K., and Bowman, C. T., in *Twenty-Sixth Symposium (International) on Combustion.* The Combustion Institute, Pittsburgh, 1996, pp. 481–488.